International Journal of Computational Intelligence Systems and Applications. Volume 10, Issue 1, (2023) 8-15
http://www.cayley-nielson.com/ijcisa/

Analysis on the Influence of Land Reclamation on Urban Heat Island Intensity in Caofeidian

Xu Chang, Xingxia Jiang, Beilei Liu, Jikun Shi, Hongtu Ma
North China University of Science and Technology, Tangshan, China

Abstract

Since the reform and opening up, urbanization has accelerated and urban land use has changed dramatically. The expansion of cities has greatly changed the structure and type of subsurface, and many natural surfaces such as water bodies and vegetation have been replaced by impervious surfaces with high thermal capacity and low albedo such as buildings and roads. The rapid development of urbanization, on the one hand, has greatly promoted the local socio-economic development, and on the other hand, has brought about a large number of problems closely related to ecological environment, among which vegetation change and urban heat island effect are the most prominent. Urban development is closely related to land expansion, and land reclamation has become an important means of urbanization in global harbor areas. Caofeidian is located in the Bohai Sea Rim, and as a future international model ecological city, the expanding urban construction, industrial construction and reclamation activities have led to huge changes in land use and thus the urban heat island effect is becoming more and more obvious.

Keywords: Temperature inversion, Reclaim land from the sea, ENVI, Heat island effect.

1. Introduction

Surface temperature is an important term in remote sensing, which deeply affects the environmental changes of the Earth, climate and various human production activities, and plays a crucial role in the energy interchange between the atmosphere and the Earth's surface, especially in the study of global climate change, agricultural production activities, urban thermal environmental changes and geological exploration activities are widely used. Surface temperature is also an important indicator for studying urban heat island.[1] Remote sensing as a non-contact, long-range detection technology is a good tool that people love to use and is increasingly popular among scientific researchers. It enables real-time monitoring of targets over a large area at the same time, which greatly reduces the workload compared to previous survey methods and is simple, easy and reliable to implement. [2-4] Moreover, the data obtained by remote sensing technology has a very high economic value, it contains many feature information, the data synthesis is particularly high, and its cost output is very different from the economic benefit, which can save us a lot of unnecessary expenses. [5]

This project uses remote sensing and GIS technology to obtain land use information, temperature image maps, and time series analysis to compare the linkage of land use heat island effect, which is very important to study the urban heat island effect in Caofeidian area, environmental protection and greening work, and the synergistic economic development of Beijing, Tianjin and Hebei in Caofeidian.

2. Main content

In this paper, we study the spatial and temporal variation of surface temperature in Caofeidian area by inversion of surface temperature on September 11, 1990, September 6, 2000, and November 5, 2010, and the main research contents of this paper are as follows:

(1) To summarize the development history of surface temperature inversion and the current status of domestic and international research.

(2) By supervised classification, different feature types are classified, and the surface temperature obtained is fitted with accuracy, compared and analyzed, and thermal infrared channels and data models suitable for inversion are obtained.

(3) Using Landsat-8 remote sensing images to perform temperature inversion using radiative transfer equation method to obtain the real surface temperature and study the spatial and temporal changes of surface temperature in Caofeidian region during 1990-2010.

(4) Extract the normalized vegetation index (NDVI), calculate the extracted surface temperature (LST), study their correlation with temperature, and analyze the spatial and temporal variation characteristics of temperature by combining the temperature inversion results.

(5) Conduct temporal and spatial analysis of the real surface temperature of different features, and verify and analyze the feasibility of the inversion results with the synchronous meteorological data of Caofeidian area.

3. Project implementation

3.1. Research methodology

There are three main surface temperature inversion algorithms: the atmospheric correction method, the single channel algorithm and the split window algorithm. The atmospheric correction method is used in this experiment. [6]

The basic principle of the atmospheric correction method is that the atmospheric influence on surface thermal radiation is first estimated, and then this atmospheric influence is subtracted from the total thermal radiation observed by the satellite sensors to obtain the surface thermal radiation intensity, which is then converted into the corresponding surface temperature. [7]

The thermal infrared radiation brightness value L_λ received by the satellite sensor consists of three parts: the upward radiation brightness $L^\uparrow$ of the atmosphere, the real radiation brightness of the ground after passing through the atmosphere to reach the satellite sensor; the energy reflected by the downward radiation of the atmosphere after reaching the ground. The expression of the thermal infrared radiation brightness value L_λ received by the satellite sensor can be written as

$$L_\lambda = [\varepsilon B(T_s) + (1-\varepsilon)L_\downarrow]\tau + L^\uparrow \tag{3-1}$$

where τ is the atmospheric transmittance in the thermal infrared band; T_s is the true surface temperature (in K); ε is the surface specific emissivity; and $B(T_s)$ is the blackbody thermal radiance. The blackbody irradiance $B(T_s)$at temperature T is equal to:

$$B(T_s) = \left[L_\lambda - L^\uparrow - \tau(1-\varepsilon)L_\downarrow\right]/\tau\varepsilon \tag{3-2}$$

$T_s$can be obtained from Planck's formula:

$$T_s = K_2/\ln[\frac{K_1}{\mathrm{B}(T_s)} + 1] \tag{3-3}$$

For Landsat-8 TIRS Band10 data, K_1 and K_2can be obtained from the "*-MTL.txt" metadata file, where$K_1 = 774.89\mathrm{W}/(m^2 \cdot \mu\mathrm{m} \cdot \mathrm{sr})$, $K_2 = 1321.08$ K

However, the algorithm requires two additional parameters: surface specific emissivity and atmospheric profile data. The former can be calculated using the NDVI threshold method, while the latter can be obtained by visiting the NASA website (http://atmcorr.gsfc.nasa.gov/) and entering the appropriate data: central latitude and longitude and other relevant elements to obtain atmospheric profile information data: transmittance τ; upward radiance$L^{\uparrow}$; downward radiance$L_{\downarrow}$.

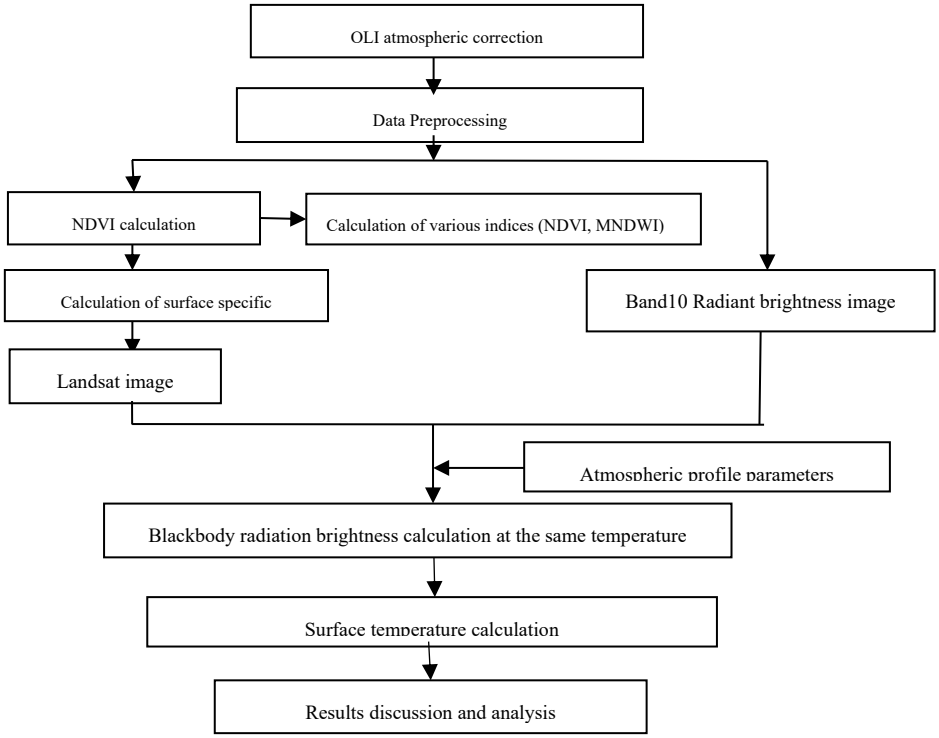

Fig. 1 Research flowchart

3.2. Research steps

(1) Learn to master various surface temperature inversion methods and determine the surface temperature inversion algorithm used in this study;

(2) Download the required remote sensing images, decompress them, perform image preprocessing, and perform radiation calibration to obtain Band10 radiation brightness images;

(3) Carry out OLI atmospheric correction and obtain various research indices (NDVI, MNDWI);

(4) The NDVI threshold method was used to obtain the surface specific emissivity;

(5) Use the preprocessed data and auxiliary parameters to calculate the blackbody radiation brightness map at the same temperature;

(6) Calculate the surface temperature according to the blackbody radiation brightness map;

(7) Combined with synchronous meteorological data in Caofeidian area to verify the accuracy, accuracy and feasibility of inversion results;

(8) Discuss and summarize.

3.3. Experimental methods

As the downloaded Landsat series data for the study area (Caofeidian area) is covered by only one view image, there is no need to mosaic and stitch the images, only geometric correction, radiometric calibration, FLAASH atmospheric correction and mask cropping processing is required.

3.4. Key technologies

3.4.1. Calculation of surface specific emissivity

Since the first band of the thermal infrared sensor is similar to the thermal infrared band of TM, this paper uses the same method as TM to calculate the specific surface emissivity.[8] That is, the NDVI threshold method is used to calculate the specific surface emissivity:

$$\varepsilon = 0.004 * P_v + 0.986 \tag{3-4}$$

In the formula, P_v is vegetation cover. P_v can be used by the following formula:

$$P_v = \left[(\mathrm{NDVI} - NDVI_{Soil})/(NDVI_{\mathrm{Veg}} - NDVI_{Soil})\right] \tag{3-5}$$

In the formula, NDVI is the normalized vegetation index.[9] $NDVI_{Soil}$ represents the NDVI value of the exposed area. $NDVI_{\mathrm{Veg}}$ represents the NDVI value of the area completely covered by vegetation. According to research, $NDVI_{\mathrm{Veg}} = 0.70$、$NDVI_{Soil} = 0.05$. When the NDVI value of a certain pixel of the image is greater than 0.70, the value of P_v is 1. P_v is 0 when the NDVI value of an image element is less than 0.05.

The NDVI image of the study area can be calculated by using the atmospheric correction results of the previous data preprocessing, which are input into ENVI 5.3 software and its NDVI tool. Then click the Band Math tool and enter the following formula to calculate the vegetation coverage image:

$$(\mathrm{B1\ gt\ 0.7}) * 1 + (\mathrm{B1\ lt\ 0.05}) * 0 + (\mathrm{B1\ ge\ 0.05\ and\ B1\ le\ 0.7}) * ((\mathrm{B1} - 0.05)/(0.7 - 0.05)) \tag{3-6}$$

In the formula, B1 is NDVI image.

Then, continuing with the Band Math tool, enter the following formula:

$$0.004 * \mathrm{B1} + 0.986 \tag{3-7}$$

In the formula, B1 is the image of vegetation coverage. And then ,the image of surface specific emissivity can be obtained by calculation.

3.4.2. Blackbody radiation brightness calculation

There is no atmospheric profile data when calculating the brightness of blackbody radiation, you can check it on the website published by NASA (http://atmcorr.gsfc.nasa.gov/), enter the corresponding data: the latitude and longitude of the center and other related content can obtain the atmospheric profile information data: transmittance τ ;Uplink spoke brightness $L^{\uparrow}$; The downlink spoke brightness $L_{\downarrow}$.

However, it should be noted that because there is no actual data on surface temperature, relative humidity, etc. The results we get are obtained by relying on the MODTRAN model [10]. The atmospheric profile data obtained by year are shown in the following table:

Table 1. Table of atmospheric profile parameters

Imaging Time	τ	Atmospheric upward radiation brightness $L^{\uparrow}$ （W/$(m^2 \times sr \times \mu m)$）	Atmospheric downward radiation brightness $L_{\downarrow}$ （W/$(m^2 \times sr \times \mu m)$）
2000/09/06	0.91	0.66	1.15
2010/11/05	0.92	0.52	0.86

Using the Band Math tool, enter the following formula:

$$\mathrm{B2} - L^{\uparrow} - \tau * (1 - \mathrm{B1}) * L_{\downarrow})/(\tau * \mathrm{B1}) \tag{3-8}$$

3.4.3. Surface temperature image calculation

After obtaining the blackbody radiation brightness image at the same temperature. You need to perform the last step to get the surface temperature image, click ENVI's Band Math tool, and enter the following formula:

$$(\mathrm{K}_2)/\mathrm{alog}(\mathrm{K}_1/\mathrm{B1} + 1) - 273 \tag{3-9}$$

In the formula, B1 is a blackbody radiant luminance image at the same temperature. K_1 and K_2 can be obtained in the metadata file. Where $K_1 = 774.89\mathrm{W}/(m^2 \cdot \mu\mathrm{m} \cdot \mathrm{sr})$, $K_2 = 1321.08$ K. Calculations can give an image of the surface temperature

3.4.4. Normalized Vegetation Index (NDVI)

Vegetation affects the energy exchange between the surface and the atmosphere at all times, and the normalized vegetation index can effectively reflect the distribution of vegetation and crop growth in the study area. In the infrared band, plants are absorbent, while in the near-infrared band, the transmittance and reflectivity of plants are large, so its spectral properties in these two bands are very different [11]. The normalized vegetation index can only represent the vegetation information of the time and place, and cannot represent the vegetation growth in a large area for a long time, and many factors such as environmental conditions will change it. It can effectively distinguish between vegetation information and non-vegetation information. Its value is generally between [-1,1]. A negative index indicates that the place is water, clouds, or other features. When the index is 0, the land is bare land. A positive index indicates that the area is green. The higher the index, the more lush the vegetation in the area. Its calculation formula is as follows:

$$\mathrm{NDVI} = \frac{(NIR-R)}{(NIR+R)} \tag{3-10}$$

In the formula, R and NIR represent the infrared band and the near-infrared band, respectively.

3.5. Study results

3.5.1. NDVI calculation results

From the above data, it can be seen that the difference between 2000 and 2010 is not significant, while the difference between 1990 and the previous two years is larger in the three-year vegetation index.

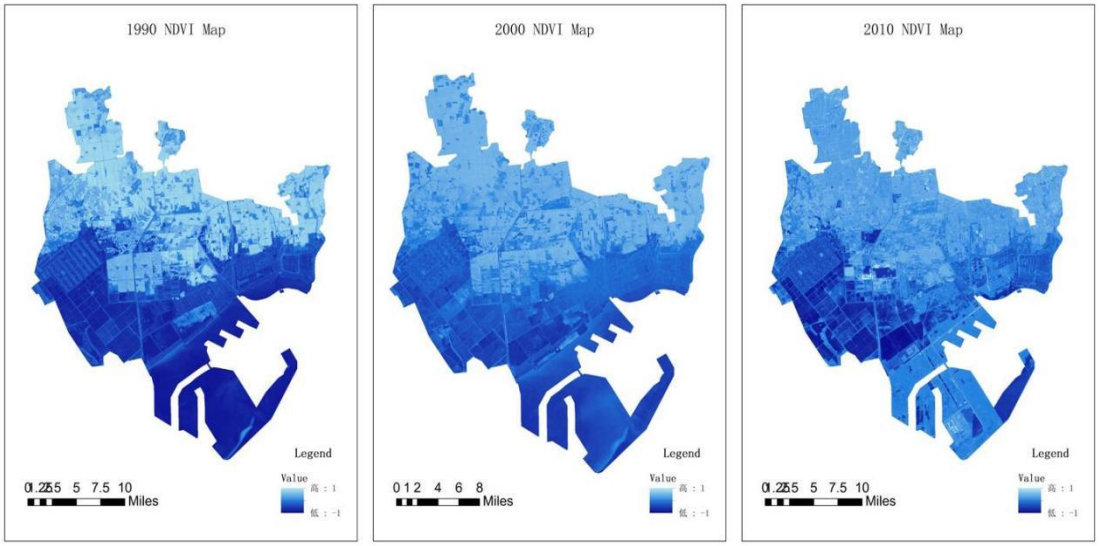

Fig. 2 NDVI maps by year

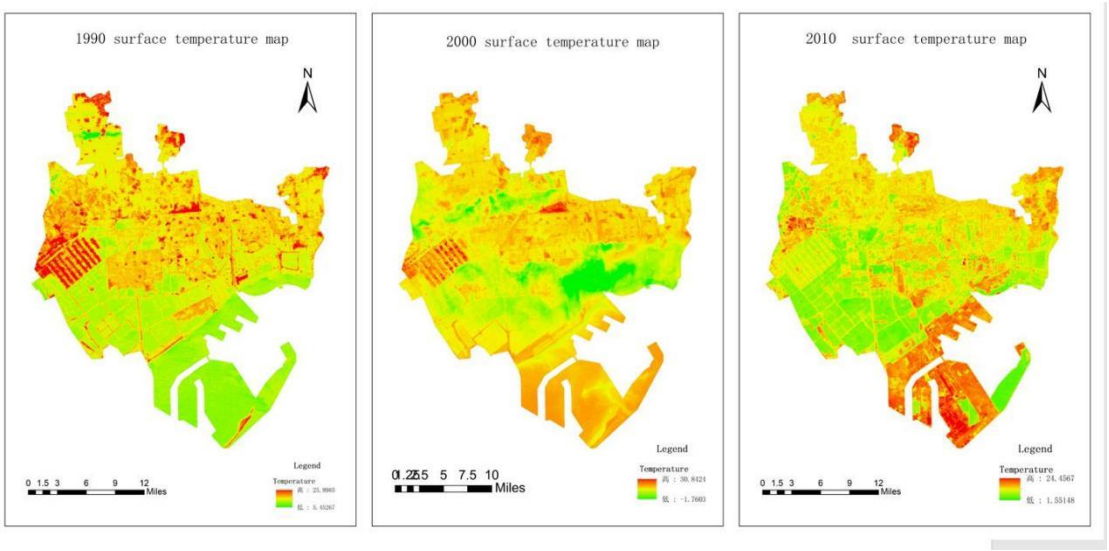

Fig. 3 Results of surface temperature inversion by year

In general, the vegetation index in the northern part of Caofeidian is high and close to 1 compared to the southern part, with lush vegetation; the vegetation index in the western edge of Caofeidian and the southeastern coastal area is close to -1; the vegetation index in the central and southern Caofeidian Industrial Zone is close to 0, with sparse vegetation.The vegetation index in the south increased in 2000 relative to 1990, probably due to a decrease in soil moisture; in 2010 relative to 2000, the vegetation index in the south increased and tended more towards 1, probably due to the decreasing area of water due to long-term land

reclamation.Overall, the vegetation index in the southern reclaimed land area gradually increases, while the northern part has a tendency to gradually decrease, which is influenced by land use changes.

3.5.2. Surface temperature image computation

According to the surface temperature calculation formula, after the color classification rendering process, the final mapping to obtain the inverse Caofeidian surface temperature image is as Fig. 3.

According to the results of the three-year inversion, it can be seen that: the temperature in the three years does not differ much from the overall, and in 1990 the temperature in the north of Caofeidian was higher than in other areas, distributed between 20 and 30°C; the temperature in the south was between 0 and 10°C and occupied most of the area. The overall temperature increase in the Caofeidian region in 2000 exceeded 30°C in some areas, mainly in the southern part of the region, accounting for roughly 25% of the overall increase, while the northern part of the region experienced an overall decrease in temperature. The overall temperature in 2010 was slightly lower, with temperatures below 25°C in the north and between 10 and 20°C in the vast majority of the area, accounting for about 70% of the total, with less than 30% of the area above 20°C, mainly in the southern part of the Caofeidian Industrial Zone.

Temporally, the overall differences in surface temperature between 1990, 2000, and 2010 were not significant, with a slight increase in overall temperature in 2000 and the lowest overall temperature in 2010. Spatially, the areas with lower temperatures in all three years are in the western corner, eastern corner, and small central area of Caofeidian. The industrial area in the south is the highest temperature area in Caofeidian due to industrial development, and its temperature is significantly higher in all four years. Because of the lush vegetation cover in the north and the industrial area in the south, the temperature in the south of Caofeidian is higher than that in the north, with no significant difference between the east and west parts.

4. Existing problems and future research ideas

There are many shortcomings in this study, mainly in:

(1) The time gap of the data selected in this study is slightly large, and it is difficult to find suitable data due to the cloud volume and time limitation of remote sensing images, which can lead to some differences in the inversion results of four years.

(2) Although the data clouds selected for the study were all below 5% and negligible, they were not de-clouded, and clouds have a large influence on the surface temperature inversion, which can lead to bias in the inversion results. At the same time, only four years 1990, 2000 and 2010 were selected to represent the 20 years from 1990-2010 to study the spatial and temporal variation characteristics of Caofeidian surface temperature, and the data are relatively small and have a certain chance. If more data are used, such as averaging multiple remote sensing images for four seasons of spring, summer, autumn and winter each year, the results will be more reliable and credible.

(3) When it comes to atmospheric profile parameters, because there is no actual surface data such as temperature and relative humidity, the final results are obtained by relying on the MODTRAN model, and the accuracy of the data can be further improved.

(4) The surface specific emissivity used in this paper is obtained by NDVI threshold method, where the accuracy of vegetation coverP_v can be further improved. A more accurate surface specific emissivity data can be obtained by dividing the surface into water bodies, urban areas and natural surfaces using the method proposed by Qin Zhihao et al.

In view of the above deficiencies and problems, it is hoped that the accuracy of the inversion can be further improved and made more accurate in future studies. Since it is impossible to obtain remote sensing data with several periods of exactly the same time, and different years are not completely comparable even at the same time, it is hoped that the inversion can be performed by averaging the surface temperature data of multiple periods when the conditions allow. There is more than one method for surface temperature inversion, and it is hoped that surface temperature inversion can be performed by different methods to compare and obtain more accurate inversion results.

References

[1] Ju-Ming Wang." Caofeidian District accelerated the integration of urban and rural education" Hebei Daily 2023-03-16,012, Local Caofeidian District.

[2] Gao Yue, Luo Li,and Li Hongyuan." Natural vegetation succession characteristics and its influencing factors in land reclamation areas of Tianjin." Soil and Water Conservation Bulletin 42.04(2022):251-257.

[3] Van Tol Zachary,and Ellis Andrew."Analysis of urban Heat Island intensity through air mass persistence: A case study of four United States cities." Urban Climate 47.(2023).

[4] Shen Chuhui, et al."Prediction of the future urban heat island intensity and distribution based on landscape composition and configuration: A case study in Hangzhou." Sustainable Cities and Society 83.(2022).

[5] Sun Yinglong, et al. "Spatial and temporal variation characteristics of heat island effect in Beijing from 2000-2019 and influencing factors." Environmental Ecology 2.08(2020):43-50.

[6] Wang Chaoyang, Song Xinxin, et al." A study on the spatial and temporal characteristics of urban heat island effect in Zhengzhou City based on MODIS data." Green Technology 24.09(2022):200-204+210.

[7] Duan Sibo, et al." Research progress on surface temperature remote sensing inversion of thermal infrared data from Landsat satellites." Journal of Remote Sensing 25.08(2021):1591-1617.

[8] Liu Xiaoyan, et al." Evaluation of multiple atmospheric correction methods in Landsat8/OLI data processing in Jiaozhou Bay." Spectroscopy and spectral analysis 42.08(2022):2513-2521.

[9] Meng Xiangchen, et al." Landsat 8 surface temperature inversion and verification: a case study of the Heihe River Basin." Journal of Remote Sensing 22.05(2018):857-871

[10] YU Shan, et al. "Spatiotemporal Changes in NDVI and Its Driving Factors in the Kherlen River Basin." Chinese Geographical Science 33.02(2023):377-392.

[11] Xiong Shiwei, et al." Application of MODTRAN model in HJ/CCD image atmospheric correction." Jiangsu Journal of Agricultural Sciences 32.02(2016):319-324.